Geophysical Research Letters

RESEARCH LETTER
10.1029/2019GL086550

Aerosol Indirect Effects on Cirrus Clouds Based on Global Aircraft Observations

Ryan Patnaude[1] **and Minghui Diao**[1]

[1]Department of Meteorology and Climate Science, San Jose State University, San Jose, CA, USA

Key Points:
- Isolating thermodynamic and dynamical effects is critical to quantify aerosol indirect effects
- IWC, Ni, and Di show positive correlations with Na when Na > 500 nm and >100 nm are 3 and 10 times higher than average, respectively
- Larger (small) aerosols are more effective at warmer (colder) *T*, indicating different nucleation mechanisms

Supporting Information:
- Supporting Information S1

Correspondence to:
M. Diao,
minghui.diao@sjsu.edu

Citation:
Patnaude, R., & Diao, M. (2020). Aerosol indirect effects on cirrus clouds based on global aircraft observations. *Geophysical Research Letters*, *46*, e2019GL086550. https://doi.org/10.1029/2019GL086550

Received 6 DEC 2019
Accepted 13 MAR 2020
Accepted article online 18 MAR 2020

Abstract Cirrus clouds have large climate impacts, yet aerosol indirect effects on cirrus microphysical properties remain highly uncertain. There is a lack of observational analysis on thermodynamic, dynamical, and aerosol indirect effects simultaneously, which limits the quantification of each effect. Using seven National Science Foundation aircraft campaigns, impacts of temperature, relative humidity, vertical velocity, and aerosols are individually quantified. Nonmonotonic correlations of ice water content, ice crystal number concentration (Ni), and mean diameter (Di) with respect to aerosol number concentrations (Na) are consistently seen at various conditions. Positive correlations become significant when Na > 500 nm (Na_{500}) and >100 nm (Na_{100}) are 3 and 10 times higher than average, respectively. While Na_{500} are more effective at temperatures closer to −40 °C with small vertical velocity fluctuations and are less sensitive to ice supersaturation, Na_{100} are more effective at colder temperatures with higher updraft and higher ice supersaturation, indicating heterogeneous and homogeneous nucleation mechanisms, respectively.

Plain Language Summary Cirrus clouds in the upper troposphere can either warm or cool the Earth surface. At temperatures ≤−40 °C, cirrus clouds are entirely composed of ice and form under two major mechanisms, depending upon the environmental conditions such as temperature, water vapor, vertical velocity, and aerosols. Ice forms with the help of a solid particle via heterogeneous nucleation, while homogeneous nucleation directly freezes liquid aerosols. Because multiple factors can affect cirrus cloud formation, a large uncertainty in understanding the individual effect is present. This study uses a large global data set of aircraft observations to better understand cirrus cloud formation. Findings indicate that controlling environmental factors is critical before investigating the aerosol indirect effects on ice clouds. Ice crystals are more populated and larger, in the presence of more aerosols. Comparing the impacts of larger and smaller aerosols, they show different effectiveness under various environmental conditions, indicating ice formation via heterogeneous and homogeneous nucleation, respectively. These results suggest that aerosols emitted by human activities very likely modify cirrus cloud properties, but their influences are nonmonotonic and depend on environmental conditions.

1. Introduction

Cirrus clouds play an important role in balancing the global radiation budget (Chen et al., 2000). When quantifying the magnitudes of shortwave and longwave radiation, the microphysical properties of ice crystals are important for determining whether the net radiative forcing produces a warming or cooling effect on Earth's surface (Liou, 1986). Ice water content (IWC), number concentration, and mean diameter of ice crystals significantly affect cloud albedo and optical depth; therefore, quantifying these microphysical properties at various temperatures is crucial for evaluating and improving ice microphysics parameterizations in global climate models.

Ice nucleation and ice microphysical properties are affected by various factors, including thermodynamic conditions (i.e., relative humidity and temperature), dynamical conditions (e.g., vertical velocity), and aerosol number concentrations and compositions. Two major formation mechanisms contribute to ice nucleation, namely, homogeneous and heterogeneous nucleation (Pruppacher & Klett, 2010). Heterogeneous nucleation requires the presence of ice nucleating particles (INPs) but can occur at a relatively lower ice supersaturations (ISS; where relative humidity with respect to ice (RHi) >100%). In addition, heterogeneous nucleation generally produces a smaller ice crystal number concentration (Ni) compared with homogeneous nucleation (Jensen et al., 2013), which subsequently affects the net radiative forcing of cirrus clouds (Lohmann & Gasparini, 2017). Previously, a series of studies based on in situ observations showed that thermodynamic and dynamical conditions have major impacts on ice microphysical properties (D'Alessandro et al., 2017; Diao, Zondlo, et al., 2013, Diao, Zondlo, Heymsfield, Avallone, et al., 2014; Diao, Zondlo, Heymsfield, & Beaton, 2014; Diao et al., 2015, 2017; Heymsfield, 1975, 2013, 2017; Krämer et al., 2009, 2016; Luebke et al., 2013, 2016; McFarquhar & Heymsfield, 1996; Schiller et al., 2008). Other laboratory experiments (Hiranuma et al., 2014) and field observations (DeMott et al., 2015) have showed that thermodynamic conditions can also affect the types and concentrations of aerosols that can be activated as INPs.

Due to the complexity of different ice nucleation mechanisms being affected by ambient conditions and the availability of INPs, there are still large uncertainties associated with the understanding of aerosol indirect effects on ice clouds as well as the estimates of their climate impacts (Fan et al., 2016; Ghan et al., 2016; Lohmann & Feichter, 2005). Previous modeling studies found relatively weak correlations between aerosol number concentration (Na) and Ni via homogeneous nucleation; that is, Ni increases by a factor of 1.3–3 with a tenfold increase of Na (Kärcher & Lohmann, 2002; Kay & Wood, 2008; Liu & Shi, 2018). Aerosol indirect effects are also affected by other conditions in global climate model simulations, including the assumption of whether INPs activate under a constant or variable RHi threshold (Kärcher & Lohmann, 2003), the inclusion of subgrid-scale vertical velocity (Penner et al., 2018; Shi & Liu, 2016; Wang et al., 2014), subgrid-scale water vapor variability (Wu et al., 2017), aerosol size distribution (Liu & Shi, 2018), and preexisting ice (Kuebbeler et al., 2014; Shi et al., 2015) in model parameterizations. To improve the understanding of aerosol indirect effects, several observation-based analyses have been conducted. Using aircraft observations, Cziczo et al. (2013) showed that mineral dust and metallic particles frequently reside in ice residuals, which are the residuals after removing water from ice particles. Field measurements of INPs show that total aerosol concentrations with diameters greater than 500 nm can be used as a good indicator of the INP number concentrations at >−36 °C (DeMott et al., 2010). A satellite-based analysis demonstrated the importance of separating stronger and weaker convection when examining aerosol indirect effects on convective and anvil clouds (Zhao et al., 2019). The authors showed that using aerosol optical depth as a proxy for aerosol loading, ice cloud effective radius (r_e) decreases with polluted continental aerosols near cloud top in strong convection but increases with aerosols in moderate convection. Up to today, there is a lack of in situ observations that studies aerosol indirect effects by simultaneously quantifying the impacts of thermodynamic and dynamical conditions. Ideally, such analysis would not only require high-resolution, accurate measurements of a series of variables such as water vapor, temperature, vertical velocity, aerosol number concentrations, and cloud hydrometeors but also relies on a significant number of samples to provide statistically robust results.

This study aims to address this knowledge gap by examining aerosol indirect effects under controlled thermodynamic and dynamical conditions, specifically temperature, RHi, and vertical velocity. A major advancement of this work is to develop a comprehensive in situ data set from several flight campaigns, covering from 87°N to 75°S, providing ample number of samples to study various ambient conditions and geographical locations. Seven flight campaigns funded by National Science Foundation (NSF) onboard the NSF/National Center for Atmospheric Research Gulfstream-V (G-V) research aircraft are used in this study. The analyses provide an unprecedented geographical coverage based on research aircraft observations, which can serve as a valuable resource for evaluating model simulations, as well as complementing other measurement techniques.

2. In Situ Data Sets and Instrumentation

For this study, 1-Hz aircraft-based observations are obtained from the NSF G-V research aircraft. A comprehensive data set is developed based on quality-controlled measurements from seven NSF flight campaigns listed in chronological order: (1) the Stratosphere-Troposphere Analyses of Regional Transport 2008 campaign (Pan et al., 2010), (2) the High-Performance Instrumented Airborne Platform for Environmental Research Pole-to-Pole Observations (HIPPO) global campaign (Wofsy et al., 2011), (3) PRE-Depression Investigation of Cloud-systems in the Tropics (Montgomery et al., 2012), (4) Tropical Ocean tRoposphere Exchange of Reactive Halogen Species and Oxygenated VOC (Volkamer et al., 2015), (5) Deep Convective Clouds and Chemistry project (Barth et al., 2015), (6) CONvective TRansport of Active Species in the Tropics (Pan et al., 2017), and (7) the O_2/N_2 Ratio and CO_2 Airborne Southern Ocean Study (Stephens et al., 2018). Due to the lack of ice particle measurements in HIPPO deployment #1, only HIPPO deployments #2–5 are included. Our data set provides a total of ~1,000 flight hours from April 2008 (Stratosphere-Troposphere Analyses of Regional Transport 2008) to February 2016 (O_2/N_2 Ratio and CO_2 Airborne Southern Ocean Study), including 84 and 423 hr of in-cloud and clear-sky conditions at temperatures ≤−40 °C, respectively. These campaigns provide an extensive spatial coverage from 87°N to 75°S and 128°E to 38°W, from the surface to the upper troposphere and lower stratosphere. The flight tracks for all seven flight campaigns used in this study are shown in Figure 1a. In-cloud frequency distributions of temperature and vertical velocity for each campaign at temperatures ≤-40 ºC are shown in Figures 1b and 1c, respectively.

Temperature measurements were collected by the Rosemount temperature probe with an accuracy and precision of ~±0.3 and 0.01 K, respectively. For this study, observations are restricted to temperature ≤−40 °C to eliminate the presence of supercooled liquid water droplets. Water vapor measurements are from the Vertical Cavity Surface Emitting Laser hygrometer (Zondlo et al., 2010), measuring at 25 Hz with an accuracy and precision of ~6% and ≤1%, respectively. Temperature and water vapor are used at 1 Hz for this analysis. Relative humidity is derived from temperature and water vapor measurements with a combined uncertainty of 6.9% to 7.8% from −40 °C to −78 °C, respectively. RHi is calculated from water vapor mixing ratio, pressure, and temperature, following the equation of saturation vapor pressure with respect to ice in Murphy and Koop (2005). The Ultra-High Sensitivity Aerosol Spectrometer uses 100 logarithmically spaced bins to measure aerosols from 0.06 to 1 μm. Ice particle measurements for all campaigns were collected using the National Center for Atmospheric Research Fast Two-Dimensional Cloud Probe (Fast-2DC), and it is the only cloud probe consistently onboard the G-V aircraft for all seven flight campaigns. The Fast-2DC has a measuring range of 25–1,600 μm, and larger particles can be mathematically reconstructed up to 3,200 μm. To alleviate the shattering effect and optical uncertainties, we exclude ice particles <62.5 μm (omitting the first two bins), while various cirrus cloud evolution phases can still be observed by using a size cutoff of 100 μm (Diao, Zondlo, Heymsfield, & Beaton, 2014). For definition of in-cloud conditions, we follow several previous studies that analyzed the G-V aircraft observations for clear-sky and in-cloud conditions (D'Alessandro et al., 2017; Diao, Zondlo, et al., 2013; Diao, Zondlo, Heymsfield, Avallone, et al., 2014, 2015, 2017) whereas in-cloud is considered when the 1-s sample of the Fast-2DC probe detects at least one ice particle (i.e., $>0\ L^{-1}$), while all the remaining data are considered clear-sky conditions.

3. Individual Impacts of Thermodynamics, Dynamics, and Aerosol Number Concentrations

Cirrus microphysical properties are examined in relation to four fundamental factors: temperature, RHi, vertical velocity (w), and Na for in-cloud conditions (Figure 2). The average IWC increases with increasing temperature, consistent with previous observational studies (Heymsfield et al., 2013; Schiller et al., 2008). The IWC–T space has also been used in Krämer et al. (2016) to classify two general types of cirrus—in situ origin and liquid origin cirrus. The average Ni does not show a clear trend with temperature. At −70 °C to −60 °C, the average and standard deviation of number-weighted mean diameter (Di) are 100 and ~100 μm, respectively, which are smaller than those at −50 °C to −40 °C (i.e., 200 and ~200 μm, respectively). The larger particles at warmer temperature are likely affected by several factors, such as heterogeneous nucleation that produces fewer yet larger ice particles, higher ice particle growth rate at higher water vapor partial pressure, and sedimentation of ice particles from above.

The relationships between ice microphysical properties and RHi are further examined (Figures 2d–2f). A key step to isolate temperature effect is to define a delta value, such as dRHi, which is the deviation of each 1-s RHi datum from the average RHi within each 1 °C bin from −40 °C to −70 °C (equation (1a)). Similarly, $d\log_{10}$(IWC), $d\log_{10}$(Ni), $d\log_{10}$(Di), $d\log_{10}(Na_{500})$, and $d\log_{10}(Na_{100})$ are defined as the differences between each 1-s datum and their respective 1 °C bin average equations (1c)–(1g)).

$$dRHi = RHi_T - \overline{RHi_T} \tag{1a}$$

$$dw = w_T - \overline{w_T} \tag{1b}$$

$$dlog_{10}(IWC) = log_{10}(IWC)_T - \overline{log_{10}(IWC)_T} \tag{1c}$$

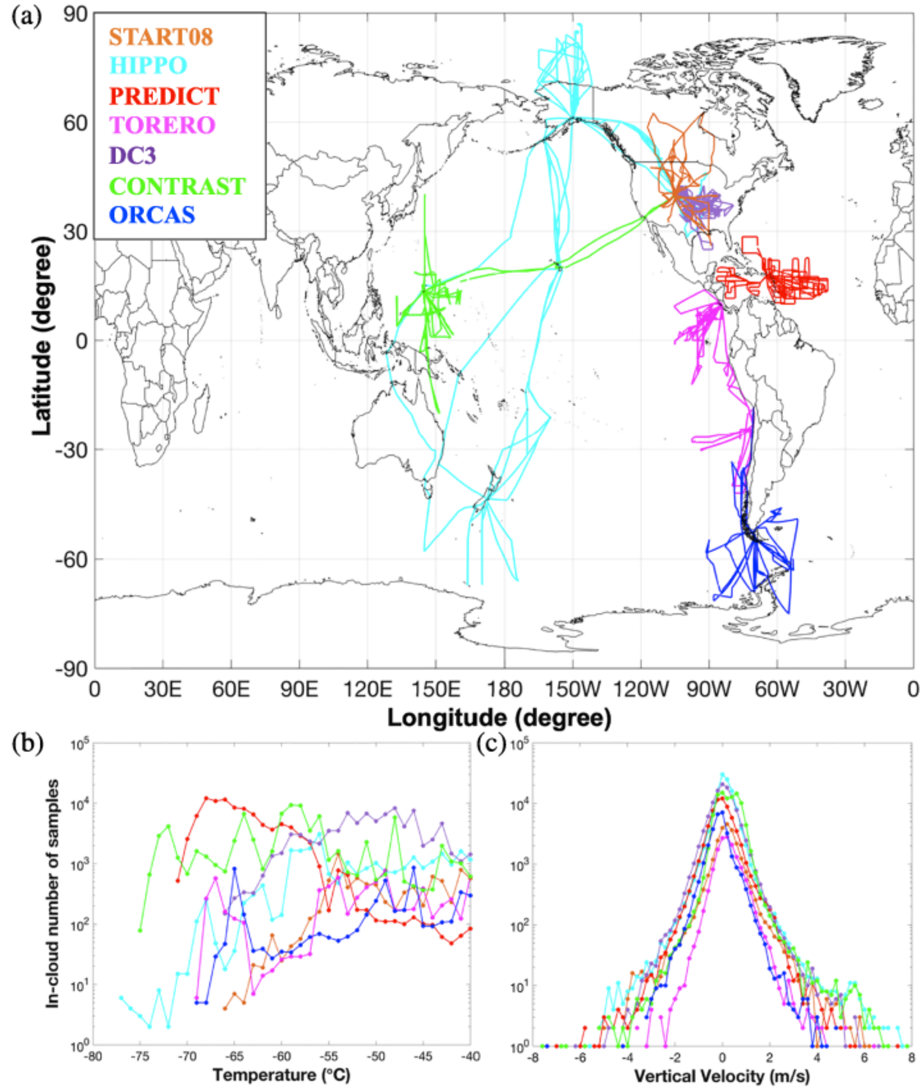

Figure 1. (a) Aircraft flight tracks of seven flight campaigns. Number of samples for (b) temperature and (c) vertical velocity at in-cloud conditions ≤−40 ºC , with colors corresponding to various flight campaigns.

$$dlog_{10}(Ni) = log_{10}(Ni)_T - \overline{log_{10}(Ni)_T} \quad (1d)$$

$$dlog_{10}(Di) = log_{10}(Di)_T - \overline{log_{10}(Di)_T} \quad (1e)$$

$$dlog_{10}(Na_{500}) = log_{10}(Na_{500})_T - \overline{log_{10}(Na_{500})_T} \quad (1f)$$

$$dlog_{10}(Na_{100}) = log_{10}(Na_{100})_T - \overline{log_{10}(Na_{100})_T} \quad (1g)$$

Here the temperature effect is mitigated by subtracting the temperature-based averages. All delta values and correlation analyses are restricted to in-cloud conditions.

The majority of the higher IWC and Ni values (i.e., $d\log_{10}$(IWC) > 0 and $d\log_{10}$(Ni) > 0, respectively) are associated with higher RHi values (dRHi > 0). When average IWC, Ni, and Di reach maximum, dRHi is at 10%, 10%, and 30%–40%, respectively. Here dRHi has a similar magnitude to ISS because the average in-cloud condition is around ice saturation. The fact that the maximum IWC, Ni, and Di do not occur at the highest RHi is mostly likely due to formation and growth of ice particles at the expense of excess water vapor over ice saturation. From ice supersaturated to subsaturated conditions, the average IWC and Ni

10.1029/2019GL086550

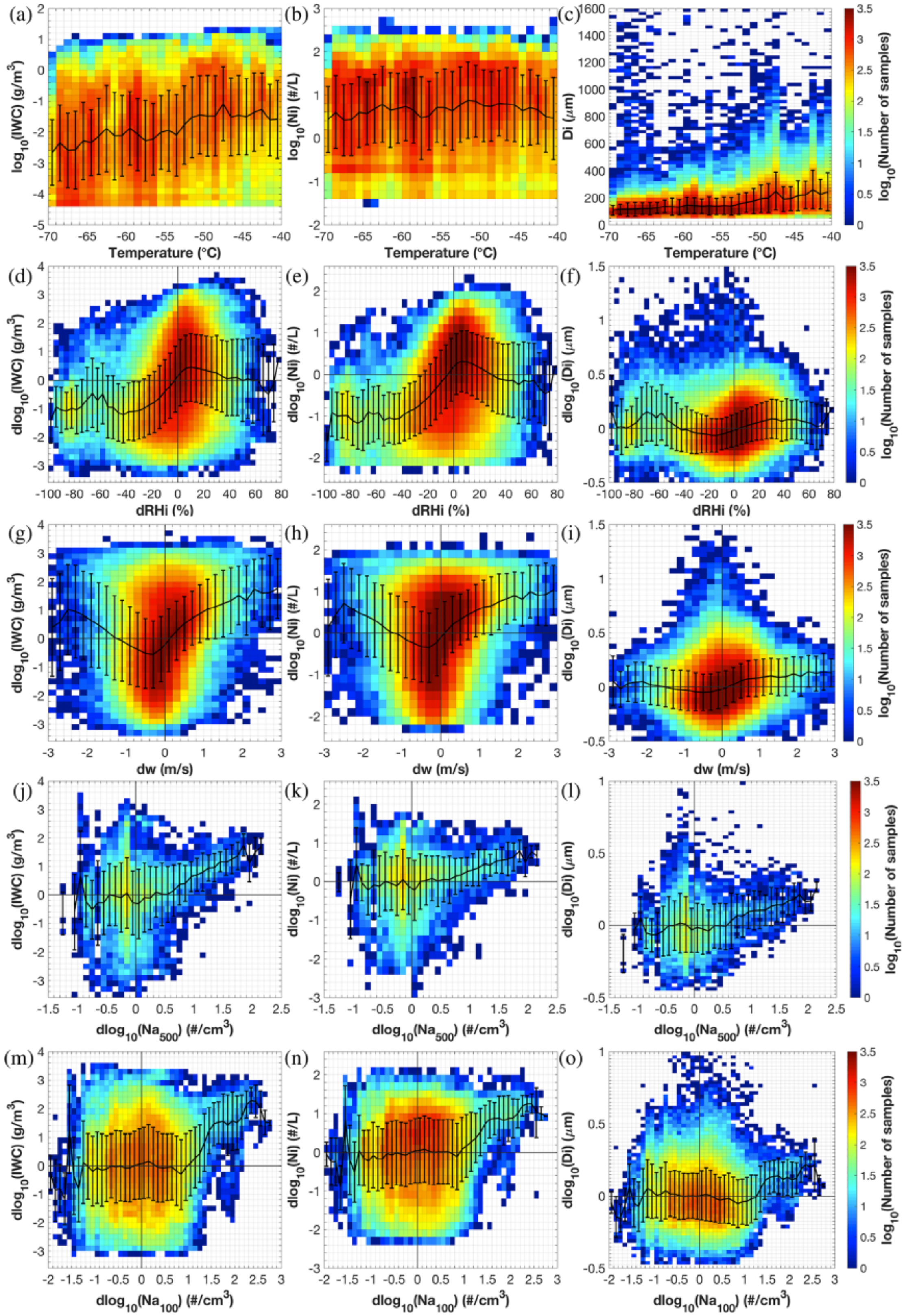

Figure 2. Distributions of IWC, Ni, and Di in logarithmic scale with respect to (a–c) temperature, (d–f) $dRHi$, (g–i) dw, (j–l) $d\log_{10}(Na_{500})$, and (m–o) $d\log_{10}(Na_{100})$. Black lines and whiskers denote averages and standard deviations, respectively.

decrease 10–30 times. The increase of Di at dryer conditions (i.e., from −20% to −70% *d*RHi) is most likely contributed by large ice particles sedimenting into subsaturated layers, which was also observed in a previous analysis of cirrus cloud evolution phases (Diao, Zondlo, et al., 2013). The large variabilities of IWC, Ni, and Di at various RHi have an important implication; that is, if aerosol indirect effects were examined without accounting for the RHi effect, the results would vary significantly depending on the RHi conditions being sampled.

Similarly, the effect of vertical velocity (w) is examined (Figures 2g–2i). The maximum and minimum IWC, Ni, and Di occur at higher updrafts ($dw > 3$ m/s) and weak downdrafts ($dw = -0.5$ m/s), respectively. The higher IWC, Ni, and Di in updrafts and downdrafts are likely due to the increasing ISS frequency in updrafts and the proximity between updrafts and downdrafts, respectively (D'Alessandro et al., 2017). Comparing the thermodynamic effect (RHi) and dynamic effect (w), the average IWC and Ni increase 1 order of magnitude when *d*RHi increases from −15% to 10%, comparable to the effect of *d*w increasing from 0 to 1 m/s.

Lastly, the correlations between cirrus microphysical properties and aerosol concentrations >500 nm (Na_{500}) and >100 nm (Na_{100}) are examined (Figure 2, last two rows). IWC, Ni, and Di are positively correlated with Na_{500}, particularly when Na_{500} is relatively higher than the average condition (i.e., $d\log_{10}(Na_{500}) > 0.5$). Similar positive correlations are also seen with respect to Na_{100}, but only when Na_{100} is 10 times higher than its average value (i.e., $d\log_{10}(Na_{100}) > 1$). The Na_{500} values are generally considered a good indicator of the number concentrations of ice nuclei facilitating heterogeneous nucleation, although those observations were limited to warmer than −36 °C (DeMott et al., 2010). The Na_{100} values are dominated by smaller aerosols, which more likely contribute to homogeneous nucleation. The fact that both Na_{500} and Na_{100} affect IWC, Ni, and Di suggest that the aerosol indirect effects in the atmosphere are effective in both pathways—heterogeneous and homogeneous nucleation. Minimizing the impacts of temperature by using the delta values is found to be an important step for analyzing aerosol indirect effects. When directly analyzing IWC, Ni, and Di (instead of their delta values) in relation to Na_{500} and Na_{100}, the positive correlations still exist but show more variabilities (Figure S1).

4. Aerosol Indirect Effects on Cirrus Clouds Under Controlled Thermodynamic and Dynamical Conditions

Aerosol indirect effects are further quantified for various ranges of temperature, *d*RHi, and *d*w (Figure 3). Specifically, geometric means of IWC, Ni, and Di in each Na bin are calculated and their linear regressions with respect to Na_{500} and Na_{100} are quantified (Table 1). Using the average ice microphysical properties inside each Na bin ensures that equal weight is assigned for each Na bin, regardless of the distribution of Na (Figure 3, last column).

Linear regressions of IWC, Ni, and Di with respect to Na_{500} show higher positive slopes of 0.743, 0.294, and 0.123 at warmer temperatures, while the slopes at colder temperatures are lower, that is, 0.453, 0.177, and 0.07, respectively. However, this trend is reversed for correlations with Na_{100}, where the highest slopes occur at the coldest temperature range. The positive correlations of IWC, Ni, and Di with respect to Na_{500} and Na_{100} are more pronounced when Na is higher, specifically when $d\log_{10}(Na_{500}) > 0.5$ and $d\log_{10}(Na_{100}) > 1$. A sensitivity test shows similar temperature effects on slope values regardless of restricting linear fits to higher Na (Figure S2). These results indicate that temperature affects the role of various aerosols in cirrus formation, with larger aerosols being more effective at warmer temperatures (possibly via heterogeneous nucleation) and smaller aerosols being more effective at colder temperatures (possibly via homogeneous nucleation). For the entire range of Na, $d\log_{10}(\mathrm{IWC})$ increases by a factor of 2.8–5.5 and 2.5–4.8 with a tenfold increase of $d\log_{10}(Na_{500})$ and $d\log_{10}(Na_{100})$, respectively (Table 1). At much higher Na, IWC increases by a factor of 10 (100) compared with temperature-based averages as Na_{500} (Na_{100}) increases from 10 to 100 times higher than its average conditions. The smaller increase of IWC with respect to Na_{500} is consistent with heterogeneous nucleation, since only a small fraction of the total Na population can be activated as ice nuclei (Rogers et al., 1998), depending on aerosol composition and morphology, etc. The larger increase in IWC with respect to smaller aerosols is consistent with homogeneous nucleation which freezes a larger fraction of the aerosol population compared with heterogeneous nucleation (Koop et al., 2000).

10.1029/2019GL086550

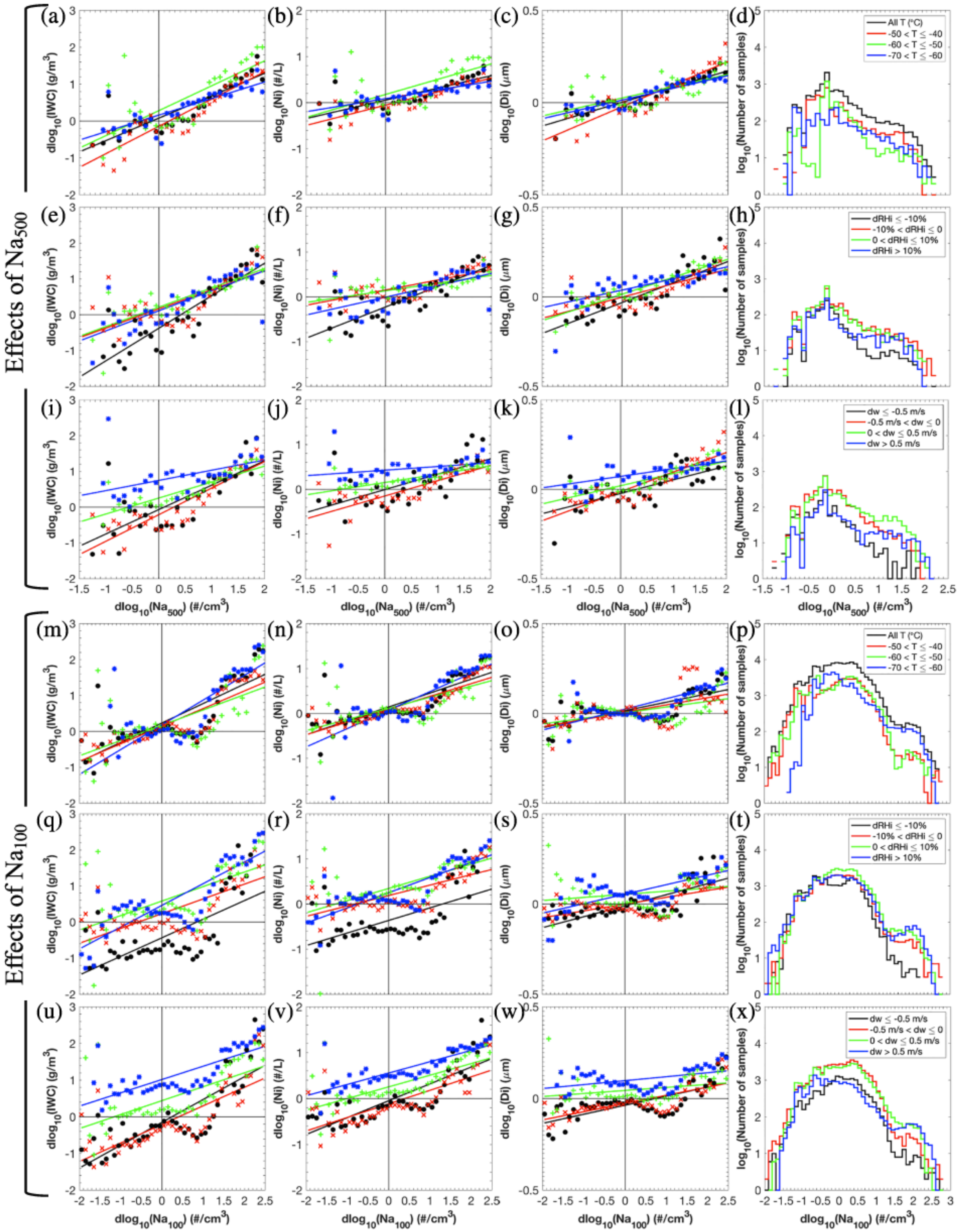

Figure 3. Linear regressions of $d\log_{10}$(IWC), $d\log_{10}$(Ni), and $d\log_{10}$(Di) with respect to $d\log_{10}(Na_{500})$ and $d\log_{10}(Na_{100})$ under controlled (a–c and m–o) temperature, (e–g and q–s) dRHi, and (i–k and u–w) dw. The last column shows number of samples for Na_{500} and Na_{100}. Markers denote the geometric means of ice microphysical properties in each Na bin.

10.1029/2019GL086550

Table 1

Linear Regressions of IWC, Ni, and Di With Respect to Na_{500} and Na_{100} Under Controlled Temperature, dRHi, and dw

		$d\log_{10}(IWC) = a + b \times d\log_{10}(Na_{500})$	$d\log_{10}(Ni) = a + b \times d\log_{10}(Na_{500})$	$d\log_{10}(Di) = a + b \times d\log_{10}(Na_{500})$	$d\log_{10}(IWC) = a + b \times d\log_{10}(Na_{100})$	$d\log_{10}(Ni) = a + b \times d\log_{10}(Na_{100})$	$d\log_{10}(Di) = a + b \times d\log_{10}(Na_{100})$
T (°C)	−70–−40	0.107 ± 0.06	0.064 ± 0.034	0.006 ± 0.008	0.255 ± 0.079	0.158 ± 0.046	0.016 ± 0.009
		0.6 ± 0.06	0.256 ± 0.034	0.086 ± 0.008	0.532 ± 0.06	0.307 ± 0.035	0.045 ± 0.007
	−50–−40	−0.106 ± 0.061	−0.04 ± 0.035	−0.017 ± 0.011	0.171 ± 0.053	0.107 ± 0.027	0.01 ± 0.012
		0.743 ± 0.061	0.294 ± 0.035	0.123 ± 0.011	0.492 ± 0.041	0.281 ± 0.021	0.042 ± 0.009
	−60–−50	0.314 ± 0.116	0.193 ± 0.072	0.027 ± 0.014	0.176 ± 0.101	0.118 ± 0.059	0.004 ± 0.01
		0.66 ± 0.119	0.332 ± 0.073	0.06 ± 0.014	0.391 ± 0.078	0.231 ± 0.046	0.026 ± 0.008
	−70–−60	0.184 ± 0.06	0.94 ± 0.039	0.017 ± 0.005	0.216 ± 0.123	0.097 ± 0.072	0.026 ± 0.012
		0.453 ± 0.061	0.177 ± 0.04	0.07 ± 0.005	0.682 ± 0.099	0.426 ± 0.059	0.049 ± 0.009
*d*RHi (%)	≤−10	−0.33 ± 0.089	−0.205 ± 0.051	−0.027 ± 0.014	−0.412 ± 0.102	−0.342 ± 0.068	−0.011 ± 0.01
		0.911 ± 0.091	0.466 ± 0.052	0.115 ± 0.014	0.508 ± 0.086	0.297 ± 0.057	0.051 ± 0.009
	−10–0	0.189 ± 0.089	0.162 ± 0.042	0.001 ± 0.011	0.242 ± 0.084	0.192 ± 0.048	0 ± 0.009
		0.523 ± 0.09	0.219 ± 0.043	0.078 ± 0.011	0.388 ± 0.064	0.219 ± 0.036	0.036 ± 0.007
	0–10	0.238 ± 0.069	0.143 ± 0.043	0.019 ± 0.008	0.592 ± 0.101	0.356 ± 0.064	0.053 ± 0.014
		0.542 ± 0.07	0.173 ± 0.044	0.098 ± 0.008	0.383 ± 0.078	0.266 ± 0.049	0.014 ± 0.011
	>10	0.139 ± 0.083	0.004 ± 0.054	0.041 ± 0.012	0.481 ± 0.079	0.262 ± 0.045	0.055 ± 0.011
		0.562 ± 0.084	0.266 ± 0.055	0.065 ± 0.012	0.581 ± 0.06	0.329 ± 0.034	0.049 ± 0.008
*d*w (m/s)	≤−0.5	−0.035 ± 0.106	0.01 ± 0.072	−0.019 ± 0.014	−0.117 ± 0.085	−0.029 ± 0.052	−0.034 ± 0.009
		0.683 ± 0.112	0.345 ± 0.076	0.077 ± 0.015	0.623 ± 0.065	0.368 ± 0.04	0.049 ± 0.007
	−0.5–0	−0.175 ± 0.069	−0.133 ± 0.049	−0.008 ± 0.01	−0.18 ± 0.083	−0.101 ± 0.054	−0.025 ± 0.008
		0.744 ± 0.07	0.343 ± 0.05	0.11 ± 0.01	0.506 ± 0.063	0.295 ± 0.041	0.045 ± 0.006
	0–0.5	0.277 ± 0.046	0.161 ± 0.024	0.024 ± 0.008	0.461 ± 0.088	0.268 ± 0.046	0.045 ± 0.011
		0.462 ± 0.047	0.181 ± 0.025	0.073 ± 0.008	0.38 ± 0.068	0.254 ± 0.036	0.017 ± 0.008
	>0.5	0.759 ± 0.091	0.43 ± 0.046	0.074 ± 0.012	1.037 ± 0.064	0.568 ± 0.035	0.099 ± 0.009
		0.257 ± 0.093	0.066 ± 0.047	0.041 ± 0.013	0.363 ± 0.05	0.247 ± 0.028	0.022 ± 0.007

Note. Intercept (a) and slope (b) are shown by the former and latter values, respectively.

For the effect of dRHi, the subsaturated condition of $d\text{RHi} \le -10\%$ shows the lowest intercepts for IWC and Ni regressions, suggesting that the average IWC and Ni are smaller by a factor of 2–10 likely due to sublimation. The aerosol indirect effect of small aerosols is more sensitive to dRHi (i.e., higher slopes at higher dRHi) than large aerosols, possibly due to a higher RHi threshold required for homogeneous nucleation.

Lastly, the correlations of IWC, Ni, and Di with respect to Na_{500} and Na_{100} are investigated under various ranges of dw (Figures 3 i–3l and 3u–3x, respectively). Higher intercepts for IWC, Ni, and Di are seen associated with higher dw, indicating higher values in strong updrafts than downdrafts or weak updrafts by a factor of 6.2 – 16.5, 3.7 – 4.7, and 1.2 – 1.4, respectively. The slope values of IWC, Ni, and Di with respect to Na_{500} decrease with increasing dw, indicating that under higher updrafts the aerosol indirect effect of large aerosols is reduced. Such dampening effect from higher updrafts is slightly weaker on the aerosol indirect effect of smaller aerosols. From downdrafts to updrafts, the slopes of Ni–Na_{500} decrease most significantly from 0.345 to 0.066, while its counterpart of Ni–Na_{100} only decreases from 0.368 to 0.247. The large dampening effect on the aerosol indirect effect from larger aerosols indicates that when sufficient cooling is available in updrafts, homogeneous nucleation becomes more viable and plays a more dominant role than heterogeneous nucleation. The decreasing slopes of Di–Na_{500} and Di–Na_{100} with increasing dw is consistent with a previous satellite-based analysis, which showed that impacts of aerosol loading on r_e are modulated by water vapor amount (Zhao et al., 2018).

5. Conclusions and Implications on Numerical Simulations

In this study, the relationships of cloud microphysical properties with respect to thermodynamics, dynamics, and aerosol sizes and concentrations are investigated using a composite in situ observation data set. The observations are based on seven flight campaigns, including samples over the Pacific Ocean, North and South America, the Southern Ocean, and the Caribbean. Using 1-Hz aircraft observations (~230-m horizontal resolution), we employ a new method to isolate specific thermodynamic and dynamical effects, prior to quantifications of aerosol indirect effects on ice microphysical properties.

Regarding thermodynamic and dynamical effects, the maximum IWC is found to be associated with warmer temperature (−40 °C), RHi slightly above ice saturation (10% dRHi), and strong updrafts ($d\text{w} > 3$ m/s). The impacts on Ni and Di are similar to those seen in IWC, except that Ni is less sensitive to temperature, and the maximum Di occurs at higher RHi (30% dRHi). These findings are consistent with studies that only analyzed one of these factors, such as Schiller et al. (2008) (temperature effect in their Figure 2), Diao, Zondlo, et al. (2013) (RHi effect in their Figure 3), and D'Alessandro et al. (2017) (w effect in their Figures 9 and 10). Our results demonstrate the necessity of controlling temperature, RHi, and w before investigating aerosol indirect effects, since these factors could either obscure or amplify the signal of aerosol indirect effects. Such approach takes advantages of synchronized, fast, and accurate in situ measurements, which often can be difficult to achieve by satellite observations due to uncertainties in retrievals (e.g., Diao, Jumbam, et al., 2013).

For aerosol indirect effects, we found nonmonotonic correlations of IWC, Ni, and Di with respect to Na_{500} and Na_{100}. That is, when Na is relatively lower, IWC, Ni, and Di are relatively constant or even slightly decrease with Na; when Na is relatively higher (i.e., $d\log_{10}(Na_{500}) > 0.5$ or $d\log_{10}(Na_{100}) > 1$), IWC, Ni, and Di increase with Na. Although the higher Na is a relatively small fraction of the total aerosol population, they were found at various geographical locations (Figure S3). The slight decrease of Ni and IWC at lower Na (i.e., anti-Twomey effect) is likely caused by competition between homogeneous and heterogeneous nucleation as shown in simulations (e.g., Spichtinger & Cziczo, 2010; Spichtinger & Gierens, 2009). This feature is more pronounced for nucleation phase (RHi > 120%; Figures S4 and S5). The robustness of the nonmonotonic correlations is further confirmed by several sensitivity tests, including comparing nucleation phase (RHi > 120%) with other cirrus evolution phases (lower RHi; Figures S4 and S5), comparing various latitudes (tropics versus higher latitudes; Figures S6 and S7), and analyzing impacts of coarser-scale Na (i.e., averaging Na_{100} and Na_{500} by every 100 s into ~23-km horizontal scale; Figures S4 and S8).

The linear regression slopes of $d\log_{10}$(Ni) with respect to $d\log_{10}(Na_{500})$ and $d\log_{10}(Na_{100})$ at various temperatures are 0.18–0.33 and 0.23–0.43, respectively (Table 1). That is, with a tenfold increase of Na_{500} and Na_{100}, Ni increases by a factor of 1.5–2.1 and 1.7–2.7 compared with temperature-based averages, respectively. These slopes are slightly lower than observations of ice particles <15 μm at $\text{Na} < 100\ \text{cm}^{-3}$ (slope of 0.58;

Seifert et al., 2004), and slightly higher than previous simulations that only considered homogeneous nucleation (slopes of 0.1–0.3; Kärcher & Lohmann, 2002; Kay & Wood, 2008; Liu & Shi, 2018). The increase of Ni and Di differs from anticorrelated Ni and Di in a single nucleation event with constant total water content. Such feature is corroborated by cirrus evolution observations (Diao, Zondlo, et al., 2013, 2014b) and simulations with continuous cooling or uplifting (Diao et al., 2017; Spichtinger & Gierens, 2009).

The role of heterogeneous and homogeneous nucleation can be speculated based on the strengths of aerosol indirect effects from larger and smaller aerosols, respectively. The effect of larger (smaller) aerosols is stronger at warmer (colder) temperature, lower (higher) RHi, and smaller (higher) w, indicating that heterogeneous nucleation is more effective when the ambient conditions do not exceed the thresholds of homogeneous nucleation. Without measurements of INP and small ice particles (<62.5 μm) for temperatures ≤−40 °C in the data set analyzed here, more investigation is warranted using other field campaigns and instrumentations. Overall, this study can be used as a blueprint for future studies to improve model parameterizations based on the observed relationships of ice microphysical properties with respect to temperature, RHi, w, and aerosol concentrations.

Acknowledgments
R. Patnaude and M. Diao gratefully acknowledge funding for this project from the NSF Division of Atmospheric and Geospace Sciences (AGS) grant 1642291 and NSF Office of Polar Programs (OPP) grant 1744965. R. Patnaude received the Walker Fellowship from San Jose State University. M. Diao acknowledges the support of the NCAR Advanced Study Program (ASP) Faculty Fellowship in 2016 and 2018. For seven NSF flight campaigns (START08, HIPPO, PREDICT, DC3, CONTRAST, TORERO, and ORCAS), we acknowledge the support from the NCAR/Earth Observation Laboratory pilots, technicians, and flight crews. M. Diao, J. DiGangi, M. Zondlo, and S. Beaton contributed to the field support, laboratory calibrations, and QA/QC of the VCSEL hygrometer. NCAR is sponsored by the National Science Foundation. We also appreciate helpful discussions with Jorgen Jensen, Stuart Beaton, and Chris Webster. All aircraft observations can be obtained at https://data.eol.ucar.edu/.

References

Barth, M. C., Cantrell, C. A., Brune, W. H., Rutledge, S. A., Crawford, J. H., Huntrieser, H., et al. (2015). The Deep Convective Clouds and Chemistry (DC3) field campaign. *Bulletin of the American Meteorological Society*, *96*(8), 1281–1309. https://doi.org/10.1175/BAMS-D-13-00290.1

Chen, T., Rossow, W. B., & Zhang, Y. (2000). Radiative effects of cloud-type variations. *Journal of Climate*, *13*(1), 264–286. https://doi.org/10.1175/1520-0442(2000)013<0264:REOCTV>2.0.CO;2

Cziczo, D. J., Froyd, K. D., Hoose, C., Jensen, E. J., Diao, M., Zondlo, M. A., et al. (2013). Clarifying the dominant sources and mechanisms of cirrus cloud formation. *Science*, *340*(6138), 1320–1324. https://doi.org/10.1126/science.1234145

D'Alessandro, J. J., Diao, M., Wu, C., Liu, X., Chen, M., Morrison, H., et al. (2017). Dynamical conditions of ice supersaturation and ice nucleation in convective systems: A comparative analysis between in situ aircraft observations and WRF simulations. *Journal of Geophysical Research: Atmospheres*, *122*, 2844–2866. https://doi.org/10.1002/2016JD025994

DeMott, P. J., Prenni, A. J., Liu, X., Kreidenweis, S. M., Petters, M. D., Twohy, C. H., et al. (2010). Predicting global atmospheric ice nuclei distributions and their impacts on climate. *Proceedings of the National Academy of Sciences*, *107*(25), 11,217–11,222. https://doi.org/10.1073/pnas.0910818107

DeMott, P. J., Prenni, A. J., McMeeking, G. R., Sullivan, R. C., Petters, M. D., Tobo, Y., et al. (2015). Integrating laboratory and field data to quantify the immersion freezing ice nucleation activity of mineral dust particles. *Atmospheric Chemistry and Physics*, *15*(1), 393–409. https://doi.org/10.5194/acp-15-393-2015

Diao, M., Bryan, G. H., Morrison, H., & Jensen, J. B. (2017). Ice nucleation parameterization and relative humidity distribution in idealized squall-line simulations. *Journal of the Atmospheric Sciences*, *74*(9), 2761–2787. https://doi.org/10.1175/JAS-D-16-0356.1

Diao, M., Jensen, J. B., Pan, L. L., Homeyer, C. R., Honomichl, S., Bresch, J. F., & Bansemer, A. (2015). Distributions of ice supersaturation and ice crystals from airborne observations in relation to upper tropospheric dynamical boundaries. *Journal of Geophysical Research: Atmospheres*, *120*, 5101–5121. https://doi.org/10.1002/2015JD023139

Diao, M., Jumbam, L., Sheffield, J., Wood, E. F., & Zondlo, M. A. (2013). Validation of AIRS/AMSU-A water vapor and temperature data with in situ aircraft observations from the surface to UT/LS from 87°N–67°S. *Journal of Geophysical Research: Atmospheres*, *118*, 6816–6836. https://doi.org/10.1002/jgrd.50483

Diao, M., Zondlo, M. A., Heymsfield, A. J., Avallone, L. M., Paige, M. E., Beaton, S. P., et al. (2014). Cloud-scale ice-supersaturated regions spatially correlate with high water vapor heterogeneities. *Atmospheric Chemistry and Physics*, *14*(5), 2639–2656. https://doi.org/10.5194/acp-14-2639-2014

Diao, M., Zondlo, M. A., Heymsfield, A. J., & Beaton, S. P. (2014). Hemispheric comparison of cirrus cloud evolution using in situ measurements in HIAPER Pole-to-Pole Observations. *Geophysical Research Letters*, *41*, 4090–4099. https://doi.org/10.1002/2014GL059873

Diao, M., Zondlo, M. A., Heymsfield, A. J., Beaton, S. P., & Rogers, D. C. (2013). Evolution of ice crystal regions on the microscale based on in situ observations. *Geophysical Research Letters*, *40*, 3473–3478. https://doi.org/10.1002/grl.50665

Fan, J., Wang, Y., Rosenfeld, D., & Liu, X. (2016). Review of aerosol–cloud interactions: Mechanisms, significance, and challenges. *Journal of the Atmospheric Sciences*, *73*, 4221–4252. https://doi.org/10.1175/JAS-D-16-0037.1

Ghan, S., Wang, M., Zhang, S., Ferrachat, S., Gettelman, A., Griesfeller, J., et al. (2016). Challenges in constraining anthropogenic aerosol effects on cloud radiative forcing using present-day spatiotemporal variability. *Proceedings of the National Academy of Sciences of the United States of America*, *113*(21), 5804–5811. https://doi.org/10.1073/pnas.1514036113

Heymsfield, A. J. (1975). Cirrus uncinus generating cells and the evolution of cirriform clouds. Part I: Aircraft observations of the growth of the ice phase. *Journal of the Atmospheric Sciences*, *32*, 799–808. https://doi.org/10.1175/1520-0469(1975)032,0799:CUGCAT.2.0.CO;2

Heymsfield, A. J., Krämer, M., Wood, N. B., Gettelman, A., Field, P. R., & Liu, G. (2017). Dependence of the ice water content and snowfall rate on temperature, globally: Comparison of in situ observations, satellite active remote sensing retrieval, and global climate model simulations. *Journal of Applied Meteorology and Climatology*, *56*, 189–215. https://doi.org/10.1175/JAMC-D-16-0230.1

Heymsfield, A. J., Schmitt, C., & Bansemer, A. (2013). Ice cloud particle size distributions and pressure-dependent terminal velocities from in situ observations at temperatures from 0° to −86 °C. *Journal of the Atmospheric Sciences*, *70*(12), 4123–4154. https://doi.org/10.1175/JAS-D-12-0124.1

Hiranuma, N., Paukert, M., Steinke, I., Zhang, K., Kulkarni, G., Hoose, C., et al. (2014). A comprehensive parameterization of heterogeneous ice nucleation of dust surrogate: Laboratory study with hematite particles and its application to atmospheric models. *Atmospheric Chemistry and Physics*, *14*(23), 13,145–13,158. https://doi.org/10.5194/acp-14-13145-2014

Jensen, E. J., Diskin, G., Lawson, R. P., Lance, S., Bui, T. P., Hlavka, D., et al. (2013). Ice nucleation and dehydration in the tropical tropopause layer. *Proceedings of the National Academy of Sciences*, *110*(6), 2041–2046. https://doi.org/10.1073/pnas.1217104110

Kärcher, B., & Lohmann, U. (2002). A Parameterization of cirrus cloud formation: Homogeneous freezing including effects of aerosol size. *Journal of Geophysical Research: Atmospheres*, *107*(D23), 4698. https://doi.org/10.1029/2001JD001429

Kärcher, B., & Lohmann, U. (2003). A parameterization of cirrus cloud formation: Heterogeneous freezing. *Journal of Geophysical Research*, *108*(D14), 4402. https://doi.org/10.1029/2002JD003220

Kay, J. E., & Wood, R. (2008). Timescale analysis of aerosol sensitivity during homogeneous freezing and implications for upper tropospheric water vapor budgets. *Geophysical Research Letters*, *35*, L10809. https://doi.org/10.1029/2007GL032628

Koop, T., Luo, B., Tsias, A., & Peter, T. (2000). Water activity as the determinant for homogeneous ice nucleation in aqueous solutions. *Nature*, *406*(6796), 611–614. https://doi.org/10.1038/35020537

Krämer, M., Rolf, C., Luebke, A., Afchine, A., Spelten, N., Costa, A., et al. (2016). A microphysics guide to cirrus clouds: Part 1—Cirrus types. *Atmospheric Chemistry and Physics*, *16*(5), 3463–3483. https://doi.org/10.5194/acp-16-3463-2016

Krämer, M., Schiller, C., Afchine, A., Bauer, R., Gensch, I., Mangold, A., et al. (2009). Ice supersaturations and cirrus cloud crystal numbers. *Atmospheric Chemistry and Physics*, *9*(11), 3505–3522. https://doi.org/10.5194/acp-9-3505-2009

Kuebbeler, M., Lohmann, U., Hendricks, J., & Kärcher, B. (2014). Dust ice nuclei effects on cirrus clouds. *Atmospheric Chemistry and Physics*, *14*, 3027–3046. https://doi.org/10.5194/acp-14-3027-2014

Liou, K.-N. (1986). Influence of cirrus clouds on weather and climate processes: A global perspective. *Monthly Weather Review*, *114*, 1167–1199. https://doi.org/10.1175/1520-0493(1986)114<1167:IOCCOW>2.0.CO;2

Liu, X., & Shi, X. (2018). Sensitivity of homogeneous ice nucleation to aerosol perturbations and its implications for aerosol indirect effects through cirrus clouds. *Geophysical Research Letters*, *45*, 1684–1691. https://doi.org/10.1002/2017GL076721

Lohmann, U., & Feichter, J. (2005). Global indirect aerosol effects: A review. *Atmospheric Chemistry and Physics*, *5*(3), 715–737. https://doi.org/10.5194/acp-5-715-2005

Lohmann, U., & Gasparini, B. (2017). A cirrus cloud climate dial? *Science*, *357*(6348), 248–249. https://doi.org/10.1126/science.aan3325

Luebke, A. E., Afchine, A., Costa, A., Grooß, J. U., Meyer, J., Rolf, C., et al. (2016). The origin of midlatitude ice clouds and the resulting influence on their microphysical properties. *Atmospheric Chemistry and Physics*, *16*(9), 5793–5809. https://doi.org/10.5194/acp-16-5793-2016

Luebke, A. E., Avallone, L. M., Meyer, J., Rolf, C., & Krämer, M. (2013). Ice water content of Arctic, midlatitude, and tropical cirrus: Part 2—Extension of the database and new statistical analysis. *Atmospheric Chemistry and Physics*, *13*(13), 6447–6459. https://doi.org/10.5194/acp-13-6447-2013

McFarquhar, G. M., & Heymsfield, A. J. (1996). Microphysical characteristics of three cirrus anvils sampled during the Central Equatorial Pacific Experiment (CEPEX). *Journal of the Atmospheric Sciences*, *53*, 2401–2423. https://doi.org/10.1175/1520-0469(1996)053,2401:MCOTAS.2.0.CO;2

Montgomery, M. T., Davis, C., Dunkerton, T., Wang, Z., Velden, C., Torn, R., et al. (2012). The Pre-Depression Investigation of Cloud-Systems in the Tropics (PREDICT) experiment: Scientific basis, new analysis tools, and some first results. *Bulletin of the American Meteorological Society*, *93*(2), 153–172. https://doi.org/10.1175/BAMS-D-11-00046.1

Murphy, D. M., & Koop, T. (2005). Review of the vapour pressures of ice and supercooled water for atmospheric applications. *Quarterly Journal of the Royal Meteorological Society*, *131*(608), 1539–1565. https://doi.org/10.1256/qj.04.94

Pan, L. L., Atlas, E. L., Salawitch, R. J., Honomichl, S. B., Bresch, J. F., Randel, W. J., et al. (2017). The Convective Transport of Active Species in the Tropics (CONTRAST) experiment. *Bulletin of the American Meteorological Society*, *98*(1), 106–128. https://doi.org/10.1175/bams-d-14-00272.1

Pan, L. L., Bowman, K. P., Atlas, E. L., Wofsy, S. C., Zhang, F., Bresch, J. F., et al. (2010). The Stratosphere-Troposphere Analyses of Regional Transport 2008 experiment. *Bulletin of the American Meteorological Society*, *91*(3), 327–342. https://doi.org/10.1175/2009BAMS2865.1

Penner, J. E., Zhou, C., Garnier, A., & Mitchell, D. L. (2018). Anthropogenic aerosol indirect effects in cirrus clouds. *Journal of Geophysical Research: Atmospheres*, *123*, 11,652–11,677. https://doi.org/10.1029/2018JD029204

Pruppacher, H. R., & Klett, J. D. (2010). *Microphysics of clouds and precipitation, Atmospheric and oceanographic sciences library* (2nd ed., Vol. 18, p. 954). Springer Netherlands, Dordrecht. https://doi.org/10.1007/978-0-306-48100-0

Rogers, D. C., DeMott, P. J., Kreidenweis, S. M., & Chen, Y. (1998). Measurements of ice nucleating aerosols during SUCCESS. *Geophysical Research Letters*, *25*, 1383–1386.

Schiller, C., Krämer, M., Afchine, A., Spelten, N., & Sitnikov, N. (2008). Ice water content of Arctic, midlatitude, and tropical cirrus. *Journal of Geophysical Research*, *113*, D24208. https://doi.org/10.1029/2008JD010342

Seifert, M., Ström, J., Krejci, R., Minikin, A., Petzold, A., Gayet, J. F., et al. (2004). Aerosol-cirrus interactions: A number based phenomenon at all? *Atmospheric Chemistry and Physics*, *4*(2), 293–305. https://doi.org/10.5194/acp-4-293-2004

Shi, X., & Liu, X. (2016). Effect of cloud-scale vertical velocity on the contribution of homogeneous nucleation to cirrus formation and radiative forcing. *Geophysical Research Letters*, *43*, 6588–6595. https://doi.org/10.1002/2016GL069531

Shi, X., Liu, X., & Zhang, K. (2015). Effects of pre-existing ice crystals on cirrus clouds and comparison between different ice nucleation parameterizations with the Community Atmosphere Model (CAM5). *Atmospheric Chemistry and Physics*, *15*(3), 1503–1520. https://doi.org/10.5194/acp-15-1503-2015

Spichtinger, P., & Cziczo, D. J. (2010). Impact of heterogeneous ice nuclei on homogeneous freezing events in cirrus clouds. *Journal of Geophysical Research*, *115*, D14208. https://doi.org/10.1029/2009JD012168

Spichtinger, P., & Gierens, K. M. (2009). Modelling of cirrus clouds: Part 2—Competition of different nucleation mechanisms. *Atmospheric Chemistry and Physics*, *9*, 2319–2334.

Stephens, B. B., Long, M. C., Keeling, R. F., Kort, E. A., Sweeney, C., Apel, E. C., et al. (2018). The O_2/N_2 Ratio and CO_2 Airborne Southern Ocean Study. *Bulletin of the American Meteorological Society*, *99*(2), 381–402. https://doi.org/10.1175/BAMS-D-16-0206.1

Volkamer, R., Baidar, S., Campos, T. L., Coburn, S., DiGangi, J. P., Dix, B., et al. (2015). Aircraft measurements of BrO, IO, glyoxal, NO_2, H_2O, O_2-O_2 and aerosol extinction profiles in the tropics: Comparison with aircraft-/ship-based in situ and lidar measurements. *Atmospheric Measurement Techniques*, *8*(5), 2121–2148. https://doi.org/10.5194/amt-8-2121-2015

Wang, M., Liu, X., Zhang, K., & Comstock, J. M. (2014). Aerosol effects on cirrus through ice nucleation in the Community Atmosphere Model CAM5 with a statistical cirrus scheme. *Journal of Advances in Modeling Earth Systems*, *6*, 756–776. https://doi.org/10.1002/2014MS000339

Wofsy, S. C. (2011). HIAPER Pole-to-Pole Observations (HIPPO): Fine-grained, global-scale measurements of climatically important atmospheric gases and aerosols. *Philosophical Transactions of the Royal Society A: Mathematical, Physical and Engineering Sciences*, *369*(1943), 2073–2086. https://doi.org/10.1098/rsta.2010.0313

Wu, C., Liu, X., Diao, M., Zhang, K., Gettelman, A., Lu, Z., et al. (2017). Direct comparisons of ice cloud macro- and microphysical properties simulated by the Community Atmosphere Model version 5 with HIPPO aircraft observations. *Atmospheric Chemistry and Physics*, *17*(7), 4731–4749. https://doi.org/10.5194/acp-17-4731-2017

Zhao, B., Liou, K.-N., Gu, Y., Jiang, J. H., Li, Q., Fu, R., et al. (2018). Impact of aerosols on ice crystal size. *Atmospheric Chemistry and Physics*, *18*(2), 1065–1078. https://doi.org/10.5194/acp-18-1065-2018

Zhao, B., Wang, Y., Gu, Y., Liou, K.-N., Jiang, J. H., Fan, J., et al. (2019). Ice nucleation by aerosols from anthropogenic pollution. *Nature Geoscience*, *12*(8), 602–607. https://doi.org/10.1038/s41561-019-0389-4

Zondlo, M. A., Paige, M. E., Massick, S. M., & Silver, J. A. (2010). Vertical cavity laser hygrometer for the National Science Foundation Gulfstream-V aircraft. *Journal of Geophysical Research*, *115*, D20309. https://doi.org/10.1029/2010JD014445